PNAS
www.pnas.org

Supplementary Information for
Vapor condensation with daytime radiative cooling

Ming Zhou[1], Haomin Song[2], Xingyu Xu[3], Alireza Shahsafi[1], Yurui Qu[1], Zhenyang Xia[1], Zhenqiang Ma[1], Mikhail A. Kats[1], Jia Zhu[4], Boon S. Ooi[5], Qiaoqiang Gan[2, *], Zongfu Yu[1, *]

1. Department of Electrical and Computer Engineering, University of Wisconsin – Madison, Madison, WI 53705, USA
2. Department of Electrical Engineering, The State University of New York at Buffalo, Buffalo, NY 14260, USA
3. School of Materials Science and Engineering, Tsinghua University, Beijing 100084, China
4. College of Engineering and Applied Sciences, Nanjing University, Nanjing 210093, China
5. Photonics Laboratory, King Abdullah University of Science and Technology (KAUST), Thala, 23955-6900, Saudi Arabia

* To whom correspondence may be addressed.

Email: qqgan@buffalo.edu or zyu54@wisc.edu

This PDF file includes:

Supplementary text
Figures S1 to S11
SI References

Supplementary Information Text

1. Steady-state model of passive condensation systems

We developed a steady-state model to calculate the condensation rate of passive condensation systems. Below we describe it in detail.

We consider a general passive condenser that operates without additional energy input. As shown in Fig. S1, air with temperature T_{vapor} and relative humidity $H_{relative}$ flows underneath the condenser at a fixed speed. Here we assume the heat exchange between air and the condenser is instantaneous.

As we discussed in the manuscript, the major cooling sources in passive condensers that operate without additional energy input are convection and radiation. The cooling power from conduction is generally small comparing to that from convection and is not considered here. The total cooling power density $q_{cooling}$ is given by

$$q_{cooling}(T_{cond}) = h_c(T_{cond} - T_{amb}) + \int d\Omega \, cos\theta \int_0^\infty d\lambda \, I_{BB}(T_{cond}, \lambda)\epsilon_{cond}(\lambda, \theta) \quad \text{(S1)}$$

Here h_c is the convective heat transfer coefficient, T_{cond} and T_{amb} are the temperature of the condenser and the ambient air, respectively. $I_{BB}(T, \lambda)$ is the spectral intensity of a blackbody at temperature *T*. $\epsilon_{cond}(\lambda, \theta)$ is the angle-dependent spectral absorptivity/emissivity of the condenser. $\int d\Omega = 2\pi \int_0^{\pi/2} d\theta$ is the angular integral over a hemisphere.

Because the condenser is emissive, it also absorbs radiation from the environment, i.e., solar radiation and atmospheric radiation. Consequently, the total heating power density at the top surface of the condenser $q_{heating}$ is given by

$$q_{heating} = \int_0^\infty d\lambda \, \epsilon_{cond}(\lambda, \theta_{sun}) \, I_{AM1.5}(\lambda) + \int d\Omega \, cos\theta \int_0^\infty d\lambda \, \epsilon_{cond}(\lambda, \theta)\epsilon_{atm}(\lambda, \theta) I_{BB}(T_{atm}, \lambda) \quad \text{(S2)}$$

The first term on the right-hand side of Eq. S2 is the incident solar power absorbed by the condenser. Here $I_{AM1.5}(\lambda)$ is the AM1.5 solar spectral irradiance. We assume the condenser is facing the Sun at a fixed angle θ_{sun}. The second term on the right-hand side of Eq. S2 is the absorbed power due to incident atmospheric radiation. The angle-dependent emissivity of the atmosphere is given by(1) $\epsilon_{atm}(\lambda, \theta) = 1 - t(\lambda)^{1/\cos\theta}$, where $t(\lambda)$ is the atmospheric transmittance in the zenith direction(2). The atmospheric radiation greatly depends on the atmospheric temperature T_{atm} as the integral $\int_0^\infty d\lambda \, \epsilon_{cond}(\lambda, \theta)\epsilon_{atm}(\lambda, \theta) I_{BB}(T_{atm}, \lambda) \sim T_{atm}^4$. However, T_{atm} greatly varies with atmosphere conditions and is typically lower than the ambient air temperature T_{amb}. Without losing generosity, here we assume the atmospheric temperature is the same as the ambient air temperature, i.e., $T_{atm} = T_{amb}$.

At the bottom surface of the condenser, as the input air flows through the condenser, it is cooled down. The vapor pressure decreases as the temperature decreases. Condensation occurs when the vapor pressure reaches the saturation vapor pressure. We approximated the saturation vapor pressure $P(T)$ at temperature *T* using the Buck equation(3):

$$P(T) = 611.21 \exp\left(\left(18.678 - \frac{T - 273.15}{234.5}\right)\left(\frac{T - 273.15}{T - 16.01}\right)\right) \quad \text{(S3)}$$

The amount of power density required for vapor condensation is given by

$$q_{vapor}(T_{cond}) = C_{V,air}u\left(T_{cond} - T_{vapor}\right) + u\Delta_{vap}\left(\frac{H_{relative}P\left(T_{vapor}\right)}{RT_{vapor}} - \frac{P(T_{cond})}{RT_{cond}}\right) \quad \text{(S4)}$$

Here $C_{V,air}$ is the specific heat capacity of air at constant volume. u is the speed of the input air flow at the air-condenser interface. *R* is the ideal gas constant. Δ_{vap} is the latent heat from vapor to liquid water(4).

At steady state, the whole system reaches thermal equilibrium, which satisfies

$$q_{cooling}(T_{cond}) - q_{heating} = q_{vapor}(T_{cond}) \quad \text{(S5)}$$

For a given ambient temperature T_{amb}, vapor temperature T_{vapor} and humidity $H_{relative}$, we can solve Eq. S5 to obtain the steady-state temperature of the condenser T_{cond}. Once we obtain T_{cond}, the condensation power q_{cond} and condensation rate W_{water} of the condenser can be calculated as

$$q_{cond} = q_{cooling}(T_{cond}) - q_{heating} \quad \text{(S6)}$$

$$W_{water} = \frac{q_{vapor}}{\Delta_{vap}} M_{water} \quad \text{(S7)}$$

where M_{water} is the molar mass of water.

To further validate our theoretical model, we predict the condensation rate of our condenser based on measured T_{in}, T_{amb} and H_{in}, and compare it to the measurement. The measurement was performed from March 10th to 11th on the roof a parking ramp of University of Wisconsin – Madison. The input air flow rate $u = 0.025\ \mathrm{m/s}$. The convective heat transfer coefficient h_c is taken to be 6 $\mathrm{Wm^{-2}K^{-1}}$ to fit the experimental data. The results are plotted in Fig. S2a. The predicted condensation rate (red curve) fits the measurement (black curve) very well. Here for simplicity, we consider nighttime condensation where the solar radiation is absent.

It is important to note that the reduced condensation rate at night is due to lower temperature of the intake air at night. First, lower temperature reduces the amount of moisture in the intake air. In our experiment, only the relative humidity of the intake air is kept steady at about 94%. The temperature of the intake air is the same as the ambient air temperature, and thus varies from day to night. Figure S2b shows the temperature and the amount of moisture (absolute humidity) in the intake air during the experimental measurement. As the temperature decreases at night, absolute humidity also decreases, leading to lower condensation rate at night.

Furthermore, lower temperature of intake air also reduces the radiative cooling power of the condenser as the condenser operates at lower temperature. Figure S2c shows the radiative cooling power of the radiative condenser at different temperatures of intake air. As the temperature decreases, the radiative cooling power also decreases, resulting in reduced condensation rate at night.

2. Experimental demonstration of integrated solar distillation systems

Here we demonstrate the condensation of vapor above ambient air temperature. The experimentally measured average condensation rate of our radiative-cooling condenser is almost 2 times that of convective condenser and commercial radiative dew condenser. Below we will describe our experiments in detail.

The elevated-temperature vapor is generated from a solar evaporation chamber as shown in Fig. S3a. The evaporation chamber consists of an insulating foam box and a floating solar absorber, which is made by a black cotton fabric on top of an insulating foam(5). The opening of the foam box is covered by polyethylene film to prevent heat losses. The evaporated vapor then was pumped from the evaporation chamber to each condenser at the same rate.

Four condensers were used in our measurement: our daytime radiative-cooling condenser, a convective condenser, a blackbody, and a commercial radiative dew condenser. These condensers are the same as we described in our manuscript. The measurements were performed in Las Vegas from 10:00 to 13:00 on February 7th, 2019. The sun's peak elevation was around 38° above horizon during the period of measurement. Due to the low ambient temperature and corresponding low radiative cooling power, the condensers were tilted ~15° toward the North. The maximum solar irradiance during the day was $\sim 700\ \mathrm{W/m^2}$ and the dew point of ambient air was around $-10\ ^\circ\mathrm{C}$. The evaporation chamber and condensers were placed in a backyard. The polyethylene covers of all condensers were exposed to sunlight. The temperature T_{out} and relative humidity H_{out} of the airflow after the condenser were measured by directly attaching temperature probes at the outlet of condenser. The amount of water contained in the output airflow were then calculated as $m_{out} = H_{out}P(T_{out})V_{in}M_{water}/R$, where $P(T)$ is the vapor pressure at temperature T, R is the ideal gas constant, and M_{water} is the molar mass of water. The vapor pressure $P(T)$ was calculated using the Buck equation(3). The condensation rate then was obtained as $W_{cond} = (m_{in} - m_{out})/A_{\mathrm{cond}}$, where m_{in} is the amount of water contained in the input air flow and A_{cond} is the area of the condensers. Here, because the blackbody does not condense vapor, we used its output airflow to approximate m_{in}. The ambient temperature during measurement is around 12 °C. The theoretical maximum condensation rate at such low temperature is ~0.1 L m^{-2} $hour^{-1}$.

Figure S3b shows the measured condensation rates of our daytime radiative condenser (red), the convective condenser (black), and the commercial radiative dew condenser (blue). Because the vapor temperature is above the ambient temperature, the convective condenser was able to condense water at an average rate of ~30 ml m^{-2} $hour^{-1}$. The commercial radiative dew condenser had similar condensation rate due to its absorption of solar radiation, which turns off the radiative cooling capability of the radiative dew condenser. In contrast, our radiative condenser repels solar radiation and thus can provide radiative cooling even in direct sunlight. The condensation rate of our radiative condenser thus was much higher than that of the convective condenser and the commercial condenser, reaching ~100 ml m^{-2} $hour^{-1}$. We further took photographs of the condensing surface at the end of experiment, which are shown in Fig. S3c. More and larger water droplets can be clearly seen on our device, indicating faster condensation rate.

3. Theoretical analysis of radiative cooling in conventional solar stills

In section 2, we showed that our daytime radiative condenser can increase the condensation rate of solar evaporated vapor. When integrating daytime radiative condenser into existing solar evaporation systems, optimization of the whole system is required to maximize efficiency and minimize system complexity and cost. Moreover, such optimization is system-specific as there are various types of solar evaporation systems. Here, we use a single-slope floating solar still as a specific example, and theoretically analyze the effect of radiative cooling for water production. In this specific case, the radiative condenser can be made on a transparent substrate instead of aluminum to allow sunlight to go into the still to evaporate water (see section 11). Our analysis shows that radiative cooling can increase the water production of solar stills by 40%. Below we will describe our analysis in detail.

As shown in Fig.S4a, a single-slope floating solar still consists of a solar absorber floating on bulk water and a condensing cover. To simplify our theoretical analysis, the following assumptions have been made:

(1) The solar absorber absorbs all solar radiation within a small depth.
(2) The condenser is transparent to the solar radiation.
(3) Heat capacity of solar absorber, condensing cover and insulating materials is neglected.
(4) The solar still is perfectly vapor leakage-proof.
(5) We only consider the steady state of the whole system.

In general, the heat balance equations for the absorber and the condenser under the above assumptions can be written as

$$q_{sun} = q_{ra} + q_{eac} + q_{cac} + q_{ab} \quad \text{(S8)}$$
$$q_{ra} + q_{eac} + q_{cac} = q_{rc} + q_{cc} \quad \text{(S9)}$$

where q_{sun} is solar radiation absorbed by the absorber.

The convective heat flux q_{cac} and evaporative heat flux q_{eac} between the absorber and condenser q_{cac} can be calculated using Dunkle's semi-empirical relation(6) as

$$q_{cac} = 0.884\left(T_a - T_c + \frac{\big(P(T_a) - P(T_c)\big)(T_a + 273.15)}{2.689 \times 10^5 - P_a}\right)^{\frac{1}{3}}(T_a - T_c) \quad \text{(S10)}$$

$$q_{eac} = 0.01623\frac{P(T_a) - P(T_c)}{T_a - T_c}q_{cac} \quad \text{(S11)}$$

where T_a and T_c are the temperatures of the absorber and condenser, respectively. $P(T)$ are the partial pressure of vapor at temperature T, which can be estimated as(7)

$$P(T) = e^{\left(25.317 - \frac{5144}{T + 273.15}\right)} \quad \text{(S12)}$$

The radiative heat flux from the absorber q_{ra} can be calculated as

$$q_{ra} = \int d\Omega\, cos\theta \int_0^{\infty} d\lambda\, \epsilon_a(\lambda,\theta)[I_{BB}(T_a,\lambda) - \epsilon_c(\lambda,\theta)I_{BB}(T_c,\lambda)] \quad \text{(S13)}$$

where σ is the Stefan-Boltzmann constant, $\epsilon_a(\lambda,\theta)$ and $\epsilon_c(\lambda,\theta)$ are angle-dependent spectral absorptivity/emissivity of water and the condenser, respectively.

We assume the bulk water underneath the floating absorber is at ambient temperature T_{amb}. The heat flux from the absorber to the bulk water q_{ab} through convection and conduction is given by

$$q_{ab} = h_{ab}(T_a - T_{amb}) \quad \text{(S14)}$$

Here h_{ab} is the heat transfer coefficient between the floating absorber and the bulk water underneath, and greatly depends on the design and materials of the floating absorber. Here we consider a floating absorber consists of a solar absorber on top of a thermal insulating foam(8). The solar absorber penetrates the foam through holes to form necessary water channels to pump the bulk water to the evaporation area. However, heat can also be conducted to the bulk water along the water channels. The heat transfer coefficient h_{ab} for such absorber therefore can be modelled as parallel resistances as

$$h_{ab} = \frac{k_w A_a + k_{ins} A_{ins}}{(A_a + A_{ins})l_{ins}} \quad \text{(S15)}$$

Here k_w and k_{ins} are the thermal conductivities of the absorber and the insulating material, respectively. Because the absorber is wet, it can be modelled as water, i.e., $k_w = 0.58\ Wm^{-1}K^{-1}$. A_a and A_{ins} are the areas of the absorber and the insulating material, respectively. l_{ins} is the thickness of the insulating foam. For a 10 mm thick insulating foam, the heat transfer coefficient h_{ab} varies from 5 to 30 $Wm^{-2}K^{-2}$ (9–13). Here, we choose $h_{ab} = 15\ Wm^{-2}K^{-1}$ for our calculation.

The convective and conductive heat flux from the condenser to surrounding environment q_{cc} is given by

$$q_{cc} = h_{cc}(T_c - T_{amb}) \quad \text{(S16)}$$

where h_{cc} is the convective and conductive heat transfer coefficient and we assume $h_{cc} = 10\ W\ m^{-2}\ K^{-1}$ throughout our calculation(14).

The radiative heat flux from the condenser to the sky q_{rc} is given by

$$q_{rc} = \int d\Omega\ cos\theta \int_0^{\infty} d\lambda\ \epsilon_c(\lambda,\theta)[I_{BB}(T_a,\lambda) - \epsilon_{atm}(\lambda,\theta)I_{BB}(T_{amb},\lambda)] \quad \text{(S17)}$$

where $\epsilon_{atm}(\lambda,\theta)$ is the angle-dependent spectral emissivity of the atmosphere. Here we assume the atmospheric temperature is the same as the ambient air temperature T_{amb}.

The water production m_{water} then can be calculated as

$$m_{water} = \frac{q_{eac}}{\Delta_{vapor}} \quad \text{(S18)}$$

where $\Delta_{vapor} = 2.26 \times 10^6\ J\ kg^{-1}$ is the latent heat of evaporation.

As an example, we solve the above heat balance equations at ambient temperature of $T_{amb} = 35\ ℃$, which are similar to experimental conditions found in literature(14). We first consider a non-radiative condenser by setting the emissivity of the condenser $\epsilon_c(\lambda,\theta) = 0$. Under the above conditions, the water production is calculated using Eq. S8-18 and is around 0.51 L m^{-2} hour^{-1}. In contrast, when we integrate the condenser with radiative cooling by setting the emissivity of the condenser $\epsilon_c(\lambda,\theta) = 1$ for $\lambda > 4\ \mu m$, the water production is increased to ~0.70 L m^{-2} hour^{-1}, a 40% enhancement comparing to non-radiative condenser (Fig. S4b).

4. **Potential benefits of radiative cooling for fin-structured convective condenser**

In this section, we provide theoretical analysis of the benefits of radiative cooling for fin-structured convective condenser. Here we focus on vapor above the ambient air temperature. For vapor at the ambient air temperature, convection does not provide any cooling effect for condensation no matter how effective it is.

As shown in Fig. S5, we consider three different fin-structured condensers that are coated with different materials with different spectral emissivity. Here, we assume the coating is thin enough such that it does not affect the heat transfer coefficient h_c between fins and the airflow. This assumption can be justified by the thermal resistance R between the fins and the airflow, which is given by

$$R = \frac{1}{h_c} = \frac{t_{coating}}{k_{coating}} + \frac{1}{h_{air}} \quad \text{(S19)}$$

where $t_{coating}$ and $k_{coating}$ are the thickness and the thermal conductivity of the coating layer. h_{air} is the convective heat transfer coefficient of air and is determined by the thermal properties of air. Typically, $\mathrm{h_{air}}$ varies from 10 to 100 $\mathrm{W/m^2K}$, and thus the resulted thermal resistance is around 0.01~0.1 $\mathrm{m^2K/W}$. In contrast, assuming a low thermal conductivity of 0.15 $\mathrm{W/mK}$, the thermal resistance of a 100 μm of PDMS is ~0.0007 $\mathrm{m^2K/W}$, much smaller than that of airflow convection. It has negligible impact on the heat transfer coefficient. In the calculations below, we assume a heat transfer coefficient of $h_c = 40\ \mathrm{W\ m^{-2}}\ ℃^{-1}$, which is much larger than the values (3~10 W m^{-2} ^{o}C^{-1}) we used in the main text for a bare plate.

The radiation from the fins is quantified by the apparent emissivity. It has been shown that the apparent emissivity of fin-structured plate is always the same or greater than the emissivity of a

bare plate(15). Here, we use the minimal apparent emissivity for fin-structured plates: the same as a bare plate.

We first consider a black-fin condenser as shown in Fig. S5. The ambient temperature T_{amb} is fixed at $T_{amb} = 30\ ℃$. Saturated vapor at a constant temperature $T_{vapor} = 45\ ℃$ and relative humidity $H_{relative} = 1$ is constantly flowing underneath the condenser at a constant rate of $u = 1\ \mathrm{m/s}$. We assume the absorptivity/emissivity of the black-fin condenser is $\epsilon_{BF}(\lambda, \theta) = 1$ for all wavelengths. These parameters then were substituted into Eq. S1-7 to obtain the condensation power. For nighttime calculation, we remove the solar irradiance $I_{AM}1.5$ in Eq. S2 since there is no solar radiation. At nighttime, the condensation power of black fins can reach almost 860 W m^{-2}. However, the black-fin condenser absorbs 1000 W m^{-2} of solar radiation and becomes an evaporator.

Next, we consider our radiative-cooling condenser, which has the same finned structure as the black-fin condenser to promote convective cooling. Compared to black fins, the fins of our radiative-cooling condenser are specifically coated such that they repel all solar radiation but emit like a blackbody outside the solar spectrum, i.e., $\epsilon_{RC}(\lambda, \theta) = 0$ for $\lambda = 0.3{\sim}4\ \mu\mathrm{m}$ and $\epsilon_{RC}(\lambda, \theta) = 1$ for $\lambda > 4\ \mu\mathrm{m}$. All the other conditions are the same as the black condenser. At nighttime, because there is no solar radiation, our radiative-cooling condenser provides the same amount of condensation power (~860 W m^{-2}) as the black condenser. At daytime, unlike the black condenser which provides no condensation power due to absorption of solar radiation, our radiative-cooling condenser can still provide ~860 W m^{-2} of condensation power.

To provide further evidence of the effectiveness of our optical coating, we also consider a condenser with white fins that also repel sunlight. However, the white fins emit much less radiation than the black fins or our fins. For a typical commercial white paint, we use an emissivity of $\epsilon_W(\lambda, \theta) = 0.2$. At nighttime, the white fins only provide ~650 W m^{-2} of condensation power due to the lower emissivity compared to black fins and our radiative-cooling fins. At daytime, although the white condenser only absorbs 20% of solar radiation, its condensation power is reduced to ~450 W m^{-2}. In other words, the radiative-cooling condenser provides 90% more cooling power than a white condenser with fins.

The performance gain is summarized in the bottom panel of Fig. S5. Radiative cooling clearly enhances the cooling power of convective Fins.

5. **Performance of radiative condenser from dry to humid climates**

Here we provide analysis of the performance of radiative condensation from dry to humid climates.

We quantify the atmospheric humidity level by using the precipitable water vapor (PWV), which is the depth of water in a column of the atmosphere if all the water vapor were precipitated as rain. The commonly used relative humidity is not a good measure as it depends on temperature and varies quickly with the attitude. The PWV in dry regions, such as Nevada(16), is usually ~1 mm, while it's around 20 mm in warm and humid regions such as Japan(16). To obtain the humidity-dependent atmospheric emissivity, we first obtain the atmospheric transmittances in the zenith direction under different PMVs from ATRAN(2). Figure S6a shows the atmospheric transmittances under PWV of 1 mm, 10 mm, and 20 mm. Under low PWV (1 mm), i.e., dry conditions, the atmosphere is highly transparent in the wavelength from 16 $\mu\mathrm{m}$ to 25 $\mu\mathrm{m}$. As the humidity level and PWV increases, the atmosphere becomes less transparent in the wavelength from 16 $\mu\mathrm{m}$ to 25 $\mu\mathrm{m}$ due to absorption of infrared radiation by water vapor. The atmospheric emissivity for a given PWV then is obtained using the relation $\epsilon_{atm}(\lambda, \theta) = 1 - t(\lambda)^{1/\cos\theta}$.

We assume the ambient temperature is 30 °C and calculate the maximum condensation rates under different PWVs and vapor temperatures. The results are plotted in Fig. S6b. Here we assume the convective heat transfer coefficient is fixed at $h_c = 10\ \mathrm{W\,m^{-2}\,K^{-1}}$. For a typical solar evaporation system, the temperature of the evaporated vapor is around 50 °C. Under such

conditions, comparing to dry climates (PWV = 1 mm), the cooling power of the radiative cooler operating under humid climates (PWV = 20 mm) will be reduced from 320 W/m^2 to 270 W/m^2. In the daytime, hot vapor can be generated through solar evaporation. As the PWV increases from 1 mm to 20 mm, the condensation rate will be reduced from ~0.77 L m^{-2} hour^{-1} to ~0.69 L m^{-2} hour^{-1}, a 10% reduction in water production. In the nighttime, water vapor is at the ambient temperature, and the condensation rate will be reduced from ~0.26 L m^{-2} hour^{-1} to ~0.17 L m^{-2} hour^{-1}, a 30% reduction in water production. The overall reduction of water production from PWV = 1 mm to PWV = 20 mm is around 2 L m^{-2}.

6. Temperature dependence of the radiative cooling power

The dependence of the radiative cooling power on the temperature of the emitter is discussed in Fig. 1d in the main text. However, here we would like to provide a more detailed discussion to clarify the temperature dependence.

To simplify the discussion, we will consider the radiative heat transfer only and ignore the convective and conductive heat transfer. First, we consider a sub-ambient radiative emitter that only emits in the atmospheric-transparency window (8 ~ 13 μm). The emissivity of the emitter in this spectral region is 1. The radiative cooling power of the emitter $P_{sub}(T_e)$ at temperature T_e can be calculated as

$$P_{sub}(T_e) = P_e^{trans}(T_e) - P_a^{trans} \tag{S20}$$

$$P_e^{trans}(T_e) = \int d\Omega\, cos\theta \int_8^{13} d\lambda\, I_{BB}(T_e, \lambda) \tag{S21}$$

$$P_a^{trans} = \int d\Omega\, cos\theta \int_8^{13} d\lambda\, I_{BB}(T_{amb}, \lambda)\epsilon_{atm}(\lambda, \theta) \tag{S22}$$

where P_e^{trans} and P_a^{trans} are the power radiated from the emitter and the atmospheric radiation absorbed by the emitter in the transparent window (8 ~ 13 μm), respectively. $I_{BB}(T, \lambda)$ is the spectral irradiance of a blackbody at temperature T. The angle-dependent emissivity of atmosphere is calculated as(1) $\epsilon_{atm}(\lambda, \theta) = 1 - t(\lambda)^{1/\cos\theta}$, where $t(\lambda)$ is the atmospheric transmittance in the zenith direction (2). We assume the atmosphere is at the ambient air temperature $T_{amb} = 20\ ℃$ throughout our calculation.

We calculate the radiative cooling power for emitters at different temperatures and plot the results as blue solid line in Fig. S7. The sub-ambient radiative emitters in most literatures are operated to cool down the emitter to sub-ambient temperature. As a result, the steady-state temperature of the emitter is at or below the ambient temperature and the radiative cooling power reported in literature is ~ 100 W/m^2. The sub-ambient radiative emitter can also be used to cool down a hot object whose temperature is above the ambient temperature, e.g., vapor at 100 °C. As such, the steady-state temperature of the emitter is higher than the ambient temperature and the radiative cooling power can reach up to ~350 W/m^2.

Next, we consider our radiative condenser, which also has unity emissivity in the transparent window as the sub-ambient radiative emitter. Compared to the sub-ambient emitter, our radiative condenser also emits in the spectral regions where the atmosphere is opaque, i.e., 4~8 μm and beyond 13 μm. The radiative cooling power of our radiative condenser then can be calculated as

$$P_{cond}(T_e) = P_{sub}(T_e) + P_e^{opaq}(T_e) - P_a^{opaq} \tag{S23}$$

$$P_e^{opaq}(T_e) = \int d\Omega\, cos\theta \left(\int_4^8 d\lambda\, I_{BB}(T_e, \lambda) + \int_{13}^{\infty} d\lambda\, I_{BB}(T_e, \lambda) \right) \tag{S24}$$

$$P_a^{opaq}(T_e) = \int d\Omega\, cos\theta \left(\int_4^8 d\lambda\, I_{BB}(T_a, \lambda)\epsilon_a(\lambda, \theta) + \int_{13}^{\infty} d\lambda\, I_{BB}(T_{amb}, \lambda)\epsilon_{atm}(\lambda, \theta) \right) \tag{S25}$$

The calculated radiative cooling power for our radiative condenser at different temperatures is plotted in Fig. S7 as red solid line. At or below the ambient temperature, the condenser absorbs more atmospheric radiation than it emits in the opaque regions (4~8 μm and beyond 13 μm). As a result, the radiative cooling power of our condenser is slightly lower than the sub-ambient emitter. However, as the temperature of emitter increases, the condenser emits more radiation than it absorbs in the opaque regions. As a result, the radiative cooling power of our condenser can reach up to ~750 W/m^2, two times that of the sub-ambient emitter.

7. Applicability of radiative condenser at different locations with different climates

Here we evaluate the applicability of our radiative condenser under different climates. 4 different locations with different climates are considered, Dubai, Singapore, Albuquerque, and Madison. Dubai has hot arid climate, Singapore has hot humid climate, Albuquerque has warm arid climate and Madison has warm humid climate. Here, we quantify the humidity level by using the precipitable water vapor (PWV). For the arid climate (Dubai and Albuquerque), we assume PWV = 1mm, and for the humid climate (Singapore and Madison), we assume PWV = 20 mm. For simplicity, we only consider the condensation rate at averaged monthly high temperature and assume a constant solar irradiance of $1000\ \mathrm{W/m^2}$ for all locations. The solar reflectance of the condenser is 93% and the convective heat transfer coefficient is fixed at $10\mathrm{W/m^2K}$. We also assume the vapor temperature is $20\ ℃$ above the monthly high temperature, a typical value found in solar evaporation systems. The condensation rates of radiative condenser are then calculated using Eq. S1-7.

Figure S8 shows the average monthly maximum temperature and the calculated condensation rates for the above 4 locations. Radiative condenser provides considerable condensation ($>$ $0.35\ \mathrm{L\ m^{-2}\ hour^{-1}}$) in all 4 locations, even in Albuquerque and Madison which have high humidity and relatively low temperature. The condensation rate can be further increased by increasing the vapor temperature, and by tilting or shading the condenser to reduce solar absorption.

8. Effect of solar reflectance on condensation rates

Higher solar reflectance always increases the condensation rate of radiative condensers, especially for vapor around ambient temperatures.

To clearly demonstrate the effect of solar reflectance, here we theoretically calculate the condensation rates of radiative condensers with different solar reflectances. The ambient air temperature and the atmospheric temperature are fixed at $T_{amb} = 20\ ℃$. The convective heat transfer coefficient is fixed at $h_c = 10\ \mathrm{W/m^2}$. The AM1.5 solar spectral irradiance is used in the calculations here. The condensation rates are then calculated using Eq. S1-7 for different solar reflectance.

Figure S9 shows the condensation rates of the radiative condensers under two different vapor conditions: ambient-temperature vapor (black solid line) and elevated-temperature vapor (red solid line). For ambient-temperature vapor, a solar reflectance higher than 90% is required for condensation. For elevated-temperature vapor, even a moderate solar reflectance of 90% can provide considerable condensation (~$0.5\ \mathrm{L\ m^{-2}\ hour^{-1}}$). By increasing the solar reflectance to 100%, the condensation rates can be increased by $0.15\ \mathrm{L\ m^{-2}\ hour^{-1}}$ for both ambient-temperature and elevated-temperature vapor.

9. Measured emissivity spectrum of the aluminized tape

Figure S10 shows the emissivity spectrum of the aluminized tape, which was measured using Fourier transform infrared (FTIR) spectroscopy. It clearly shows that the aluminized tape is not emissive and thus does not contribute to cooling.

10. Solar transparent radiative condenser

To integrate our daytime radiative condenser with traditional solar distillation systems, the radiative condenser can be made on a transparent substrate instead of the aluminum plate to allow sunlight to go into the chamber to evaporate water. Here we give an example of solar transparent radiative condenser.

Figure S11a shows the schematic of the solar transparent radiative condenser. It consists of a thin layer of PDMS with a thickness of 100 μm, on top of glass. Figure S11b shows the transmission (red curve) and emissivity (black curve) spectra of the PDMS-glass condenser. 93% transmission is obtained for sunlight while a near-unity emissivity in the mid-IR is maintained.

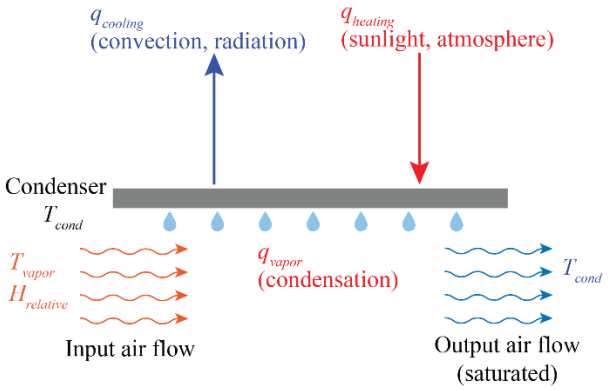

Fig. S1. Schematic of the heat balance in a passive radiative condenser.

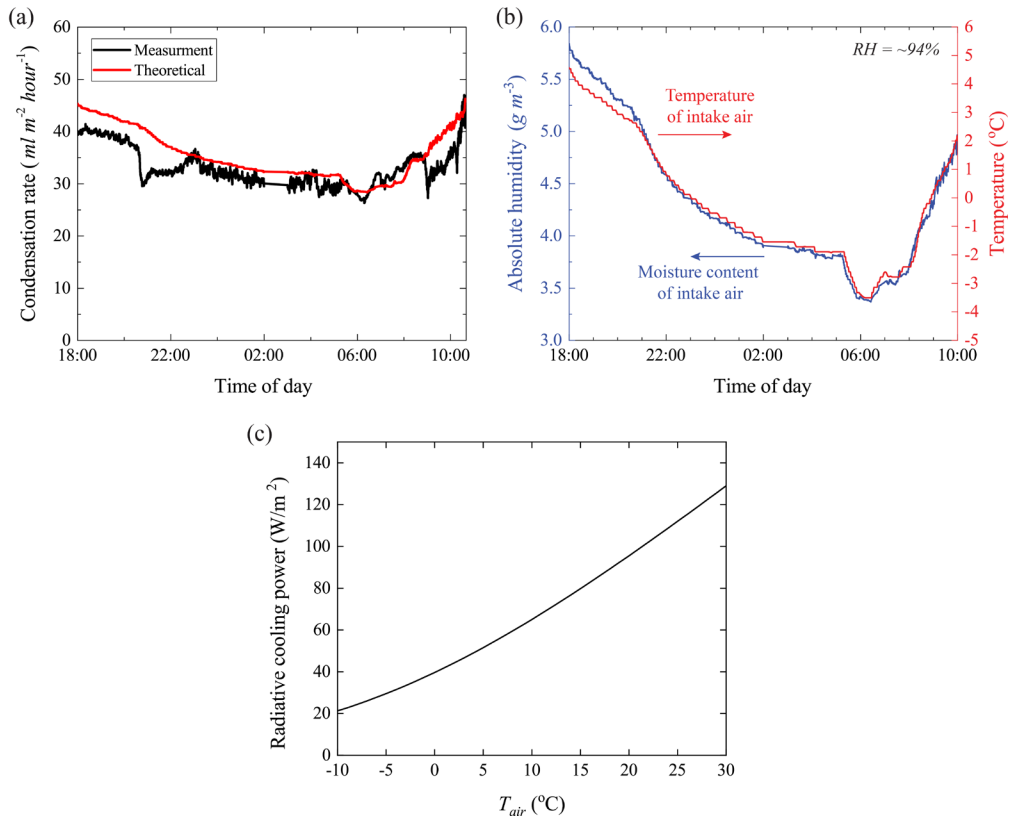

Fig. S2. (a) The theoretically predicated nighttime condensation rate (red) fits the experimental measurements (black) very well. (b) Measured temperature and moisture content of the intake air for the experiment in (a). The relative humidity of the intake air was kept steady at about 94%. The absolute humidity of the intake air decreased at night due to decreased temperature. (c) Radiative cooling power of the radiative condenser at different temperatures of the intake air. Lower temperature at night leads to reduced radiative cooling power.

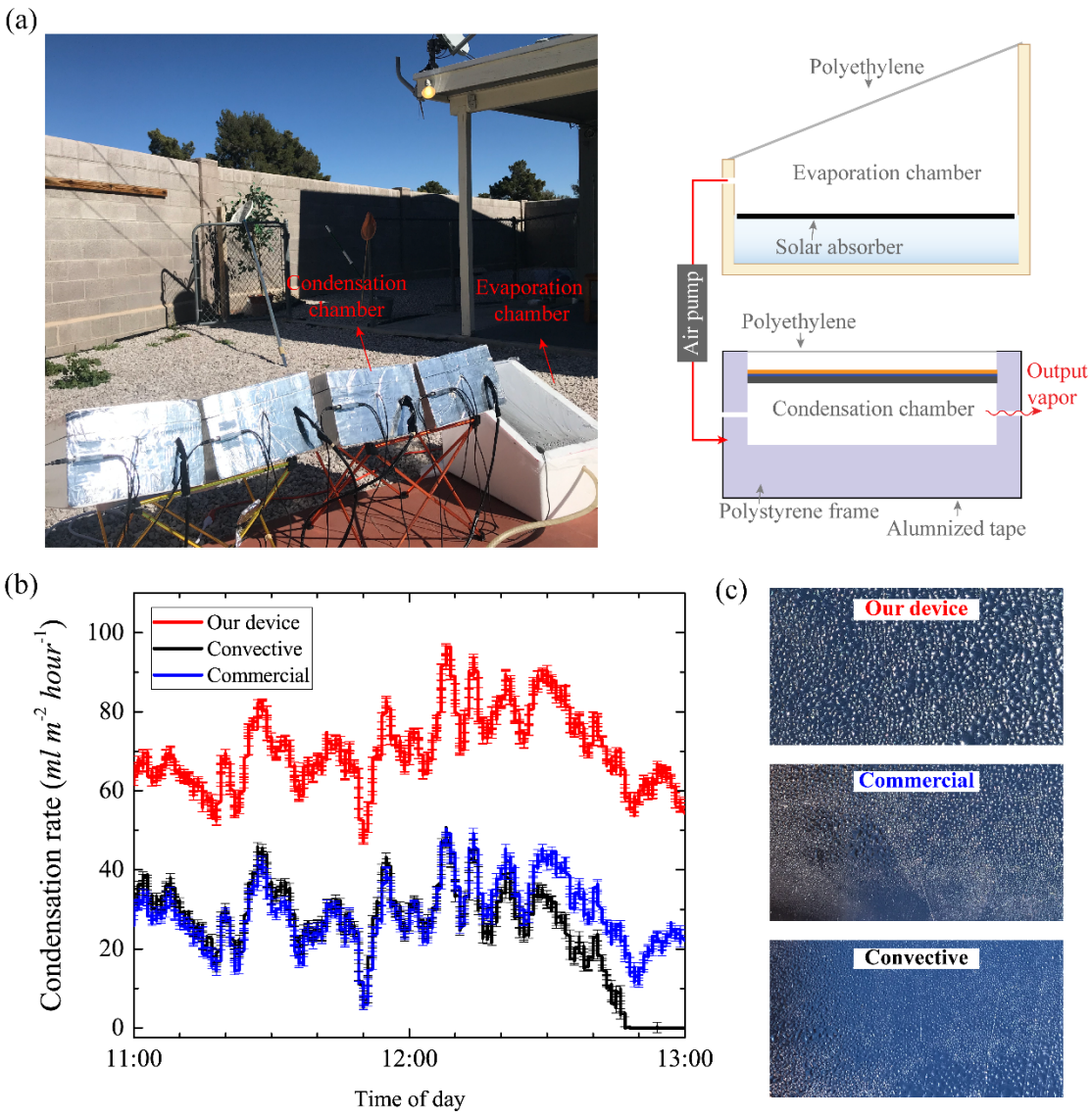

Fig. S3. (a) Left side: photograph of our outdoor experimental setup. Ride side: schematic of the experimental setup. The condensers and the evaporation chamber are placed in a backyard of a house in Las Vegas, Nevada in February of 2019. The polyethylene covers of all condensers were exposed to sunlight. (b) Real-time condensation rates of our radiative cooling condenser (red), the convective condenser (black) and the commercial radiative dew condenser (blue). (c) Photographs of the condensing surface at the end of experiment. Larger and more droplets can be clearly seen on our device, indicating faster condensation rate.

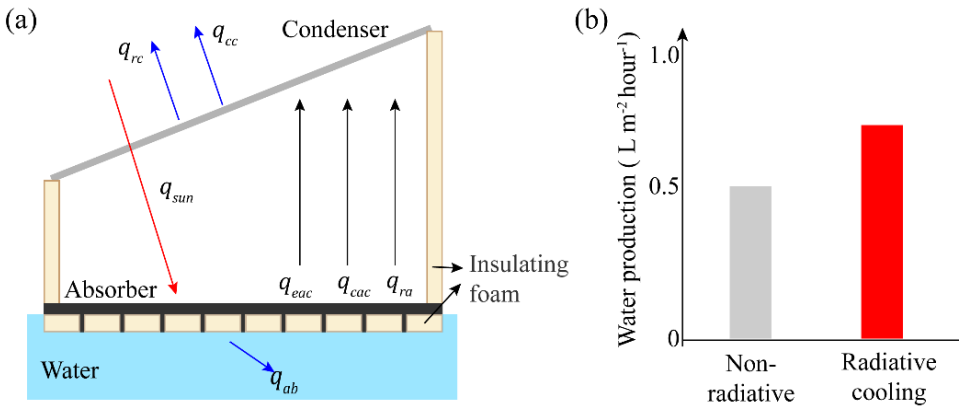

Fig. S4. (a) Schematic of a single-slope floating solar still. For simplicity, the collection of condensed water is not visualized. (b) Water production rates of the solar still with a non-radiative condensing cover (gray) and a radiative-cooling condensing cover (red). By using radiative cooling, the water production rate can be increased by 40%.

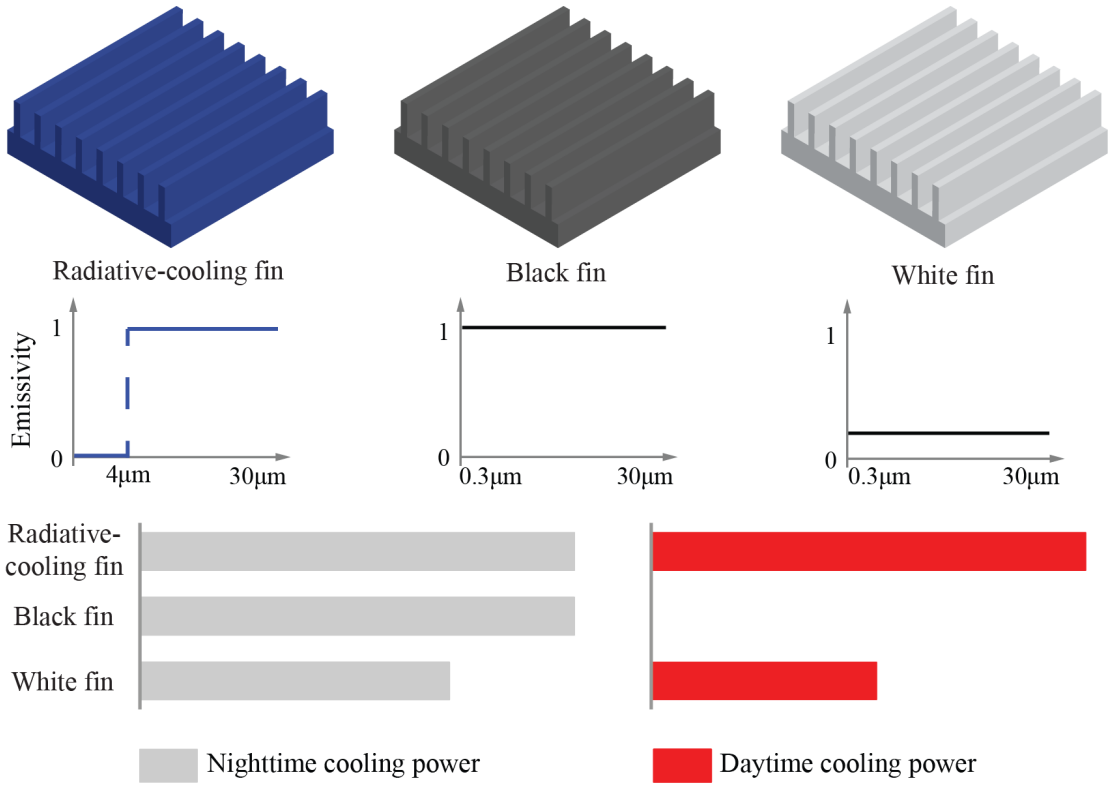

Fig. S5. Top row: condensers with radiative-cooling fins, black fins and white fins. All the fins have the same structures to enhance convective heat transfer. Middle row: spectral emissivity of the condensers. The radiative fins have a spectral emissivity of 1 beyond 4 μm wavelength. The black fins have a spectral emissivity of 1 over the entire spectrum. The white fins have an emissivity of 0.2 over the entire spectrum. Bottom row: nighttime (gray bar) and daytime (red bar) condensation power of the condensers. We assume the ambient temperature is 35 °C and vapor at temperature of 45 °C is constantly flowing underneath the condenser. The radiative-cooling fins does not absorb sunlight and can provide 1400 W m^{-2} of condensation power at both nighttime and daytime. The black fins also provide 1400 W m^{-2} of cooling power at nighttime. However, because the black fins absorb all solar radiation, their condensation power is significantly suppressed to 400 W m^{-2} in daytime. On the other hand, the white fins absorb only 20% of sunlight, but they also emit less radiation. As a result, the white fins only provide 1000 W m^{-2} of condensation power at nighttime and 800 W m^{-2} of condensation power at daytime.

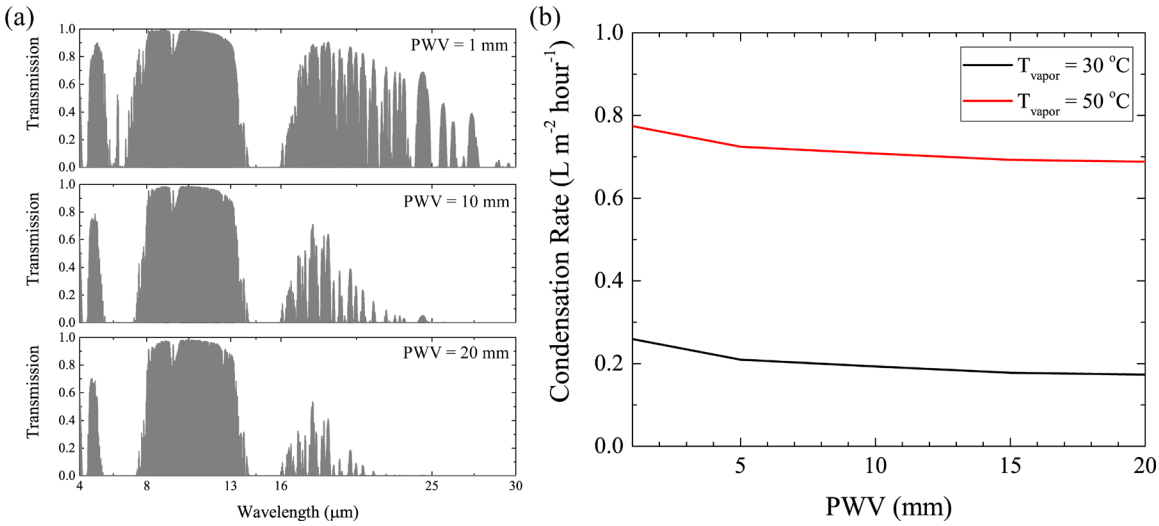

Fig. S6. (a) Atmospheric transmittances under precipitable water vapor (PWV) of 1 mm (top), 10 mm (middle) and 20 mm (bottom). Under low PWV (1 mm), i.e., dry climate, the atmosphere is highly transparent in the wavelength 16~25 μm. Under warm and humid climate, i.e., PWV > 10 mm, the atmosphere becomes highly absorptive in the wavelength 16~25 μm. (b) Maximum condensation rate of radiative condenser under different PWVs for vapor with different temperature. The ambient temperature is assumed to be 30 °C. In the daytime, the vapor temperature in a typical solar evaporation system is around 50 °C. As the PWV increases from 1 mm to 20 mm, the condensation rate reduces from ~0. 77 L m^{-2} $hour^{-1}$ to ~0.69 L m^{-2} $hour^{-1}$ (red solid line). In the nighttime, the vapor is at the ambient temperature, the condensation rate reduces from ~0. 26 L m^{-2} $hour^{-1}$ to ~0.17 L m^{-2} $hour^{-1}$ (black solid line) as the PWV increases.

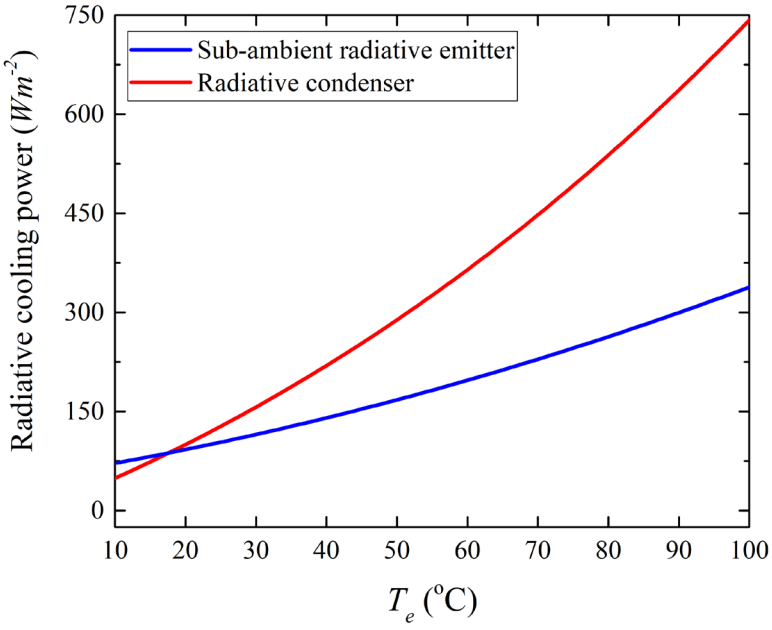

Fig. S7. Temperature dependence of the radiative cooling power for the sub-ambient radiative condenser (blue solid line) and our radiative condenser (red solid line). The sub-ambient emitter only emits from 8 ~ 13 μm. The radiative cooling power of the sub-ambient emitter is ~100 W/m^2 at the ambient temperature (20 °C), and reaches up to ~350 W/m^2 when the temperature of the emitter is 100 °C. In contrast, our radiative condenser emits in wavelengths longer than 4 μm. When the temperature of the emitter is below the ambient temperature, the radiative condenser provides less radiative cooling power than the sub-ambient emitter due to absorption of atmospheric radiation. However, at higher temperatures of the emitter, the radiative condenser provides up to two time of radiative cooling power than the sub-ambient emitter, reaching ~750 W/m^2 at 100 °C.

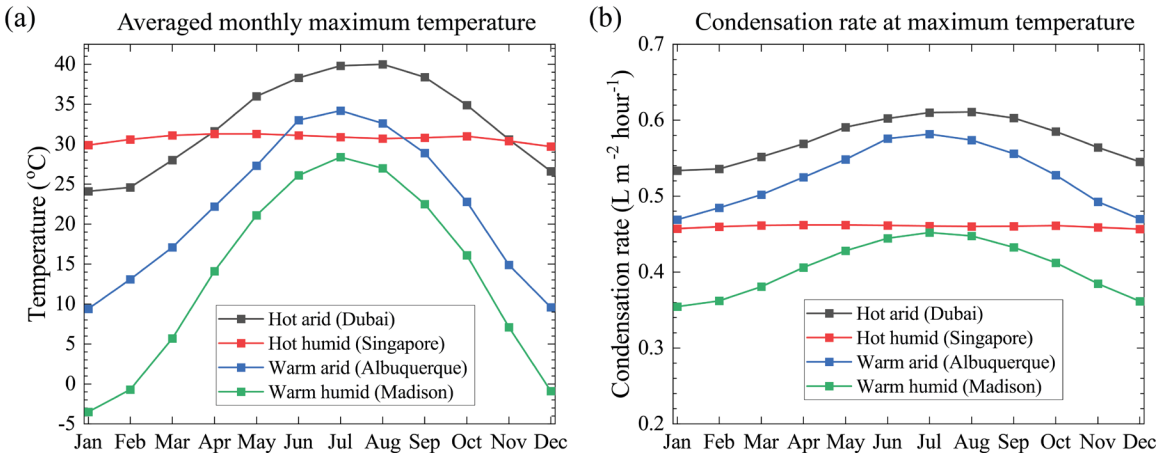

Fig. S8. (a) Average monthly maximum temperature at 4 different locations with 4 different climates, hot arid, hot humid, warm arid and warm humid. (c) Theoretically calculated condensation rates of our radiative condenser under 4 different climates.

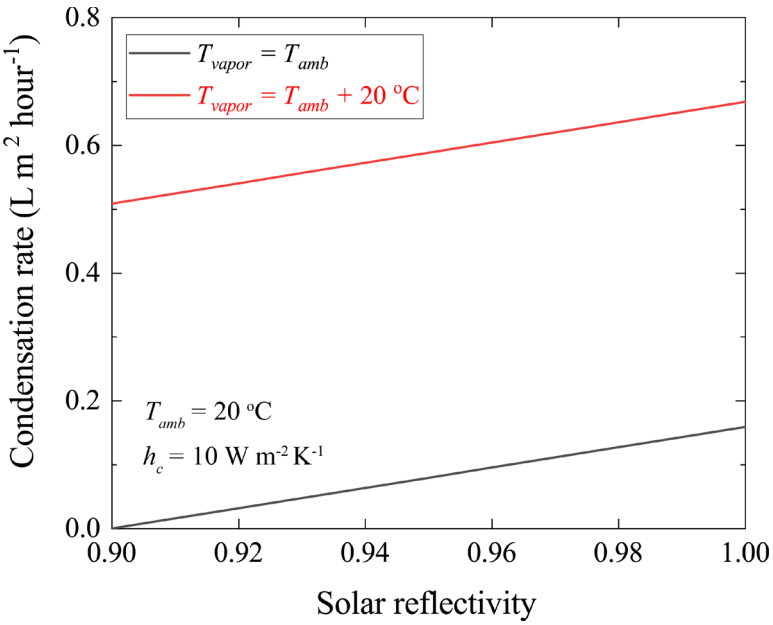

Fig. S9. Condensation rates of radiative condensers with different solar reflectance. The ambient temperature is 20 ℃ and the convective heat transfer coefficient is fixed at $10\ \mathrm{W/m^2}$. Two different vapor conditions are considered, ambient-temperature vapor and elevated-temperature vapor. For the elevated-temperature vapor, we assume the vapor temperature is 20 ℃ above the ambient temperature, i.e., 40 ℃.

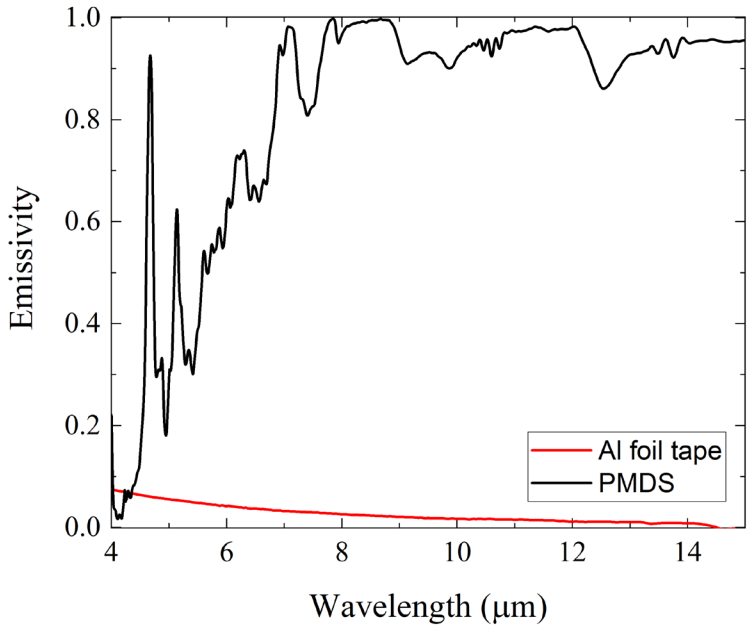

Fig. S10. Measured emissivity spectra for the aluminized tape (red line) and the PDMS layer (black line). The aluminized tape has low emissivity compared to the PDMS layer.

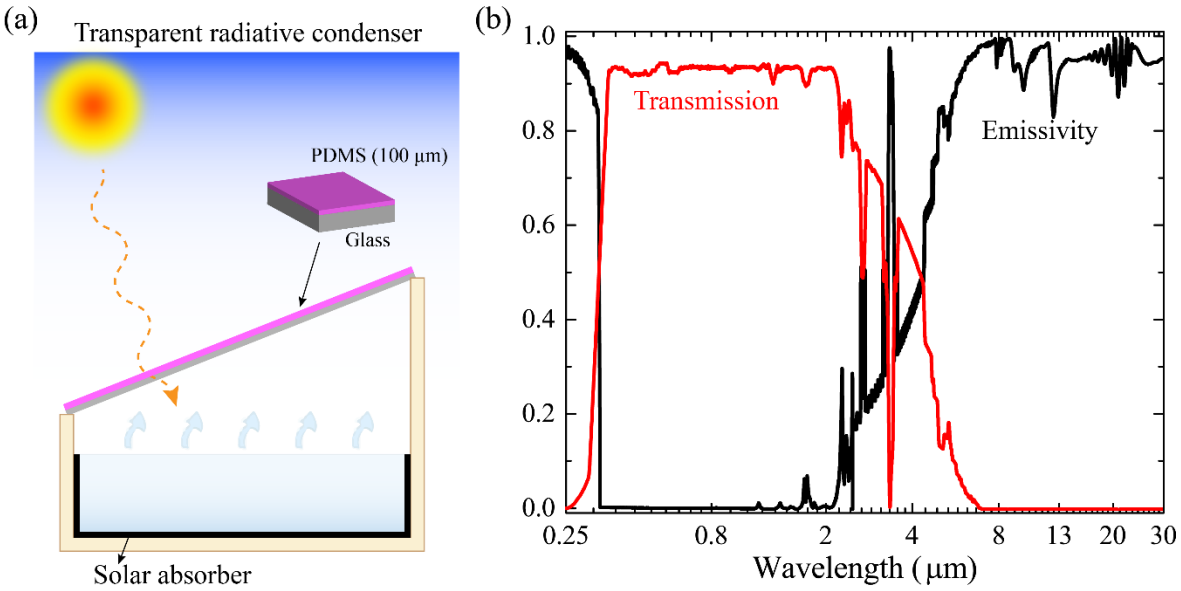

Fig. S11. (a) Schematic of transparent radiative condenser. It consists of a layer of PDMS with a thickness of 100 μm, on top of a glass. The transparent condenser can be readily implemented in existing solar stills. (b) Transmission (red) and emissivity (black) spectra of the transparent radiative condenser.

SI References

1. C. G. Granqvist, A. Hjortsberg, Radiative cooling to low temperatures: General considerations and application to selectively emitting SiO films. *Journal of Applied Physics* **52**, 4205–4220 (1981).

2. S. D. Lord, “A new software tool for computing Earth’s atmospheric transmission of near- and far-infrared radiation” (1992) (April 23, 2018).

3. A. L. Buck, New Equations for Computing Vapor Pressure and Enhancement Factor. *J. Appl. Meteor.* **20**, 1527–1532 (1981).

4. N. S. Osborne, H. F. Stimson, D. C. Ginnings, *Measurements of heat capacity and heat of vaporization of water in the range 0 degrees to 100 degrees C* (National Bureau of Standards, 1939) (February 24, 2021).

5. Z. Liu, *et al.*, Extremely Cost-Effective and Efficient Solar Vapor Generation under Nonconcentrated Illumination Using Thermally Isolated Black Paper. *Global Challenges* **1**, 1600003 (2017).

6. R. V. DUNKLE, Solar Water Distillation : The Roof Type Still and a Multiple Effect Diffusion Still. *Proc. International Heat Transfer Conference, University of Colorado, U.S.A.* **5**, 895 (1961).

7. M. K. Gaur, G. N. Tiwari, Optimization of number of collectors for integrated PV/T hybrid active solar still. *Applied Energy* **87**, 1763–1772 (2010).

8. G. Wei Ni, *et al.*, A Salt-Rejecting Floating Solar Still for Low-Cost Desalination. *Energy & Environmental Science* (2018) https:/doi.org/10.1039/C8EE00220G (March 20, 2018).

9. H. Ghasemi, *et al.*, Solar steam generation by heat localization. *Nature Communications* **5**, 4449 (2014).

10. Y. Liu, *et al.*, A Bioinspired, Reusable, Paper-Based System for High-Performance Large-Scale Evaporation. *Advanced Materials* **27**, 2768–2774 (2015).

11. Q. Jiang, *et al.*, Bilayered Biofoam for Highly Efficient Solar Steam Generation. *Advanced Materials* **28**, 9400–9407 (2016).

12. C. Jia, *et al.*, Rich Mesostructures Derived from Natural Woods for Solar Steam Generation. *Joule* **1**, 588–599 (2017).

13. F. Jiang, *et al.*, Lightweight, Mesoporous, and Highly Absorptive All-Nanofiber Aerogel for Efficient Solar Steam Generation. *ACS Appl. Mater. Interfaces* **10**, 1104–1112 (2018).

14. S. K. Shukla, V. P. S. Sorayan, Thermal modeling of solar stills: an experimental validation. *Renewable Energy* **30**, 683–699 (2005).

15. A. D. Kraus, A. Bar-Cohen, *Design and Analysis of Heat Sinks*, 1st edition (Wiley-Interscience, 1995).

16. G. G. Amenu, P. Kumar, NVAP and Reanalysis-2 Global Precipitable Water Products : Intercomparison and Variability Studies. *Bull. Amer. Meteor. Soc.* **86**, 245–256 (2005).